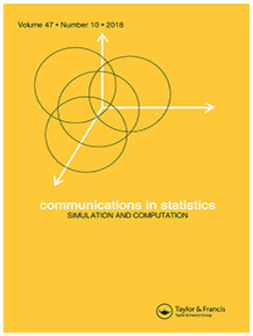

Taylor & Francis
Taylor & Francis Group

Communications in Statistics - Simulation and Computation

ISSN: 0361-0918 (Print) 1532-4141 (Online) Journal homepage: https://www.tandfonline.com/loi/lssp20

Signal discrimination without denoising

Ferebee Tunno & Miranda Perry

To cite this article: Ferebee Tunno & Miranda Perry (2019): Signal discrimination without denoising, Communications in Statistics - Simulation and Computation, DOI: 10.1080/03610918.2019.1657449

To link to this article: https://doi.org/10.1080/03610918.2019.1657449

Published online: 03 Sep 2019.

COMMUNICATIONS IN STATISTICS - SIMULATION AND COMPUTATION®
https://doi.org/10.1080/03610918.2019.1657449

Signal discrimination without denoising

Ferebee Tunno and Miranda Perry

Department of Mathematics and Statistics, Arkansas State University, Jonesboro, Arkansas, USA

ABSTRACT

This article reveals that two previously established tests for autocovariance equality between stationary autoregressive moving average (ARMA) processes can also be used to discriminate between harmonic signals embedded in noise without the need for any reconstruction or modeling. A third test is also introduced and used for the same purpose. An application involving functional magnetic resonance imaging (fMRI) as well as an extension involving a generalized linear chirp (GLC) process are presented at the end.

ARTICLE HISTORY
Received 25 September 2017
Accepted 15 August 2019

KEYWORDS
Signal plus noise; Autocovariance; fMRI; Linear chirp

1. Introduction

Consider the process

$$\{X_t\}$$

defined by

$$X_t = \sum_{i=1}^{m} A_i \sin(\lambda_i t + a_i) + Z_t \quad t = 0, \pm 1, \pm 2, \ldots \tag{1}$$

where A_i, a_i, and λ_i are constants for all $i = 1, 2, \ldots, m$ and $\{Z_t\} \sim \mathrm{WN}(0, \sigma^2)$. This is a standard *harmonic signal plus noise* model. Figure 1 shows two examples of such a process.

In practice, one is typically interested in extricating the signal from the noise. That is, the noise is viewed as a contaminating force from which the signal needs to be freed so that it can be properly understood. A wide variety of techniques exist for such "denoising" and include moving average filters, exponential smoothing, Savitsky-Golay smoothing, and Nyquist-Shannon sampling.

In addition to signal extraction, the practitioner is often interested in grouping or clustering signals into categories based on whether their waveforms are similar or dissimilar. See, for example, Mezer et al. (2009). Such signal discrimination can be done by analyzing either covariance structures in the time domain or spectral structures in the frequency domain. Kullback-Liebler and Chernoff information measures are often employed. See, Kakizawa, Shumway, and Taniguchi (1998) for a more thorough discussion.

CONTACT Ferebee Tunno ftunno@astate.edu Department of Mathematics and Statistics, P.O. Box 70, State University, Arkansas State University, Jonesboro, Arkansas 72467.

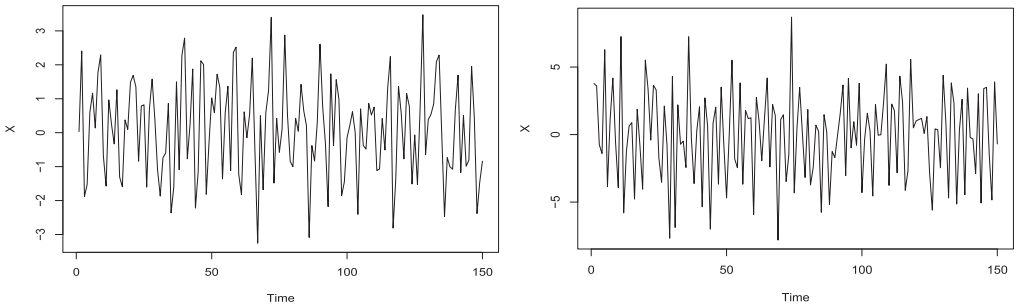

Figure 1. 150 observations from (left) $X_t = \sin t - \sin(2t) + Z_t$ with $\{Z_t\} \overset{\text{iid}}{\sim} \text{N}(0,1)$ and (right) $X_t = 2\sin(3t) - 3\cos(2t) + Z_t$ with $\{Z_t\} \overset{\text{iid}}{\sim} \text{N}(0,4)$.

This article presents three pairwise discrimination tests that do not require any signal reconstruction or model analysis. Details of these tests are outlined in the next section while various simulations appear in Sec. 3. Section 4 presents an application involving functional magnetic resonance imaging and Sec. 5 closes the article with some remarks and extensions.

2. The tests

There are three signal discrimination tests outlined in this section, all of which are designed to compare and contrast the autocovariances between two independent, stationary autoregressive moving average (ARMA) processes. Recall that if $\{A_t\} \sim \text{ARMA}(p,q)$, then

$$A_t - \sum_{i=1}^{p} \phi_i A_{t-i} = \epsilon_t + \sum_{j=1}^{q} \theta_j \epsilon_{t-j} \quad t = 0, \pm 1, \pm 2, \ldots \tag{2}$$

where $\{\epsilon_t\} \sim \text{WN}(0, \sigma_A^2)$, $\phi(z) = 1 - \phi_1 z - \cdots - \phi_p z^p$ and $\theta(z) = 1 + \theta_1 z + \cdots + \theta_q z^q$ have no common factors, and the roots of $\phi(z)$ all fall outside of the unit circle.

We now wish to apply these tests to harmonic signals embedded in noise. Such a move is natural since stationary ARMA processes can often be approximately described by harmonic signal plus noise models and vice versa. For example, in Figure 2, we see 100 observations from processes $\{A_t\}$ and $\{X_t\}$, where $\{A_t\} \sim \text{ARMA}(2,2)$ with

$$A_t - 1.72A_{t-1} + 0.99A_{t-2} = \epsilon_t - 1.37\epsilon_{t-1} + 0.72\epsilon_{t-2}$$

and $\{X_t\}$ follows (1) with

$$X_t = 3.57\cos\left(\frac{\pi t}{6} + \pi\right) + Z_t.$$

Both $\{\epsilon_t\}$ and $\{Z_t\}$ are iid standard normal. The two paths traced out in the plots are very similar. For more examples and details of this approximation process, see Sec. 4.1 of Woodward, Gray, and Elliott (2012).

In general, if $\{X_t\}$ follows (1), then its mean and autocovariance functions are given by

$$\text{E}(X_t) = \sum_{i=1}^{m} A_i \sin(\lambda_i t + a_i) \quad \text{and} \quad \text{Cov}(X_t, X_{t+h}) = \begin{cases} \sigma^2 & h = 0 \\ 0 & h \neq 0 \end{cases},$$

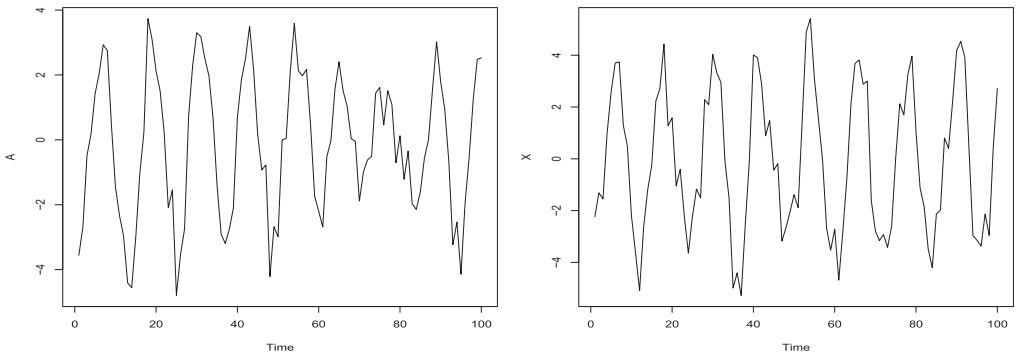

Figure 2. 100 observations from (left) $A_t - 1.72A_{t-1} + 0.99A_{t-2} = \epsilon_t - 1.37\epsilon_{t-1} + 0.72\epsilon_{t-2}$ and (right) $X_t = 3.57\cos\left(\frac{\pi t}{6} + \pi\right) + Z_t$. Both $\{\epsilon_t\}$ and $\{Z_t\}$ are iid standard normal.

respectively. Observe that since the mean depends on t, $\{X_t\}$ is not stationary (in the wide sense). However, because on the average the sine waves in question spend as much time above the time axis as they do below, it will suit our purposes to treat the process as being mean-zero. Observe also that all signals have the same autocovariance structure, and so we won't technically be discriminating between autocovariances but rather between general wave structures. Thus, if $\{X_t\}$ and $\{Y_t\}$ both follow (1) and are independent of one another, we will be testing

$$\begin{array}{l} H_0 : \{X_t\} \text{ and } \{Y_t\} \text{ have the same wave structure} \quad \text{vs.} \\ H_1 : \{X_t\} \text{ and } \{Y_t\} \text{ have different wave structures.} \end{array} \tag{3}$$

Put another way, we wish to test whether or not $\{X_t\}$ and $\{Y_t\}$ are driven by the same type of signal.

2.1. Bounded area test

Observe the scatterplot of an arbitrary mean-zero process shown in Figure 3. Typically, one "connects the dots" for better presentation as shown in Figure 4. The shaded region between these line segments and the time axis shown in Figure 5 is simply called the *bounded area*.

If $\{X_t\}$ is a time series observed at times $t = 1, 2, \ldots, n$, then the magnitude of its bounded area is equal to

$$U_n^X = \sum_{t=2}^{n} \left[\int_{t-1}^{t} |(X_t - X_{t-1})(u - t) + X_t| du \right] = \sum_{t=2}^{n} I_t^X,$$

where I_w^X is the magnitude from $t = w-1$ to $t = w$. Tunno (2015) showed that if two independent, stationary, mean-zero ARMA processes with finite second moments are observed over the same period, then a significant difference between their bounded area magnitudes implies a significant difference between their autocovariance structures.

Now assume that $\{X_t\}$ follows (1). If we treat $\{X_t\}$ as being mean-zero, then the process is stationary, which makes $\{I_t^X\}$ stationary as well. Thus, we have

$$\text{Var}(U_n^X) = \text{Var}\left(\sum_{t=2}^{n} I_t^X \right) = (n-1)\gamma_{I^X}(0) + 2\sum_{h=1}^{n-2}(n - 1 - h)\gamma_{I^X}(h),$$

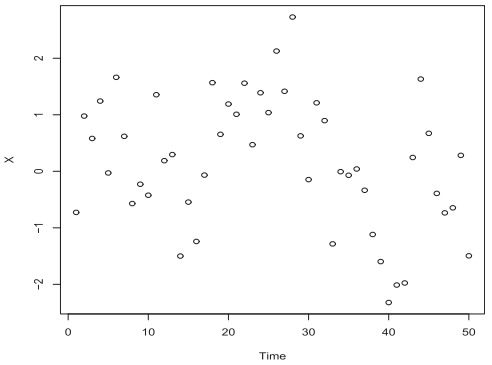

Figure 3. A scatterplot of an arbitrary mean-zero time series.

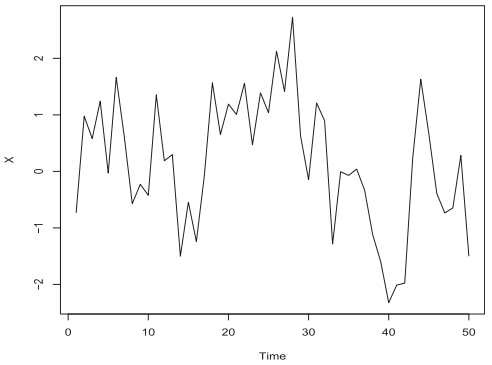

Figure 4. The same scatterplot from Figure 3, but with line segments connecting adjacent points.

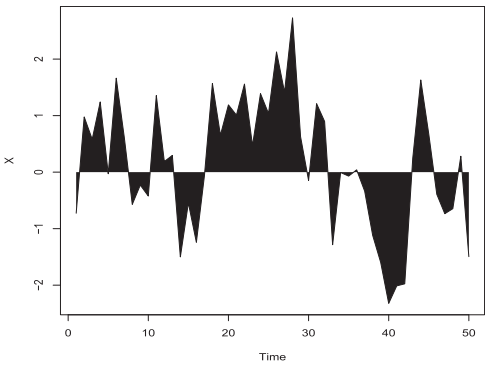

Figure 5. The shaded region between the line segments and the time axis is referred to as the *bounded area*.

where $\gamma_{I^X}(h) = \text{Cov}(I_t^X, I_{t+h}^X)$. If $\{Y_t\}$ also follows (1), then U_n^Y and its associated functionals are defined analogously.

If $\{X_t\}$ and $\{Y_t\}$ are independent of one another, then given samples $X_1, X_2, \ldots, X_n$ and $Y_1, Y_2, \ldots, Y_n$, a normalized test statistic for (3) is equal to

$$T_1 = \frac{U_n^X - U_n^Y - \text{E}(U_n^X - U_n^Y)}{\sqrt{\text{Var}(U_n^X - U_n^Y)}} = \frac{U_n^X - U_n^Y - \left(\text{E}(U_n^X) - \text{E}(U_n^Y)\right)}{\sqrt{\text{Var}(U_n^X) + \text{Var}(U_n^Y)}}.$$

Under the assumptions that the null hypothesis in (3) implies $\mathrm{E}(U_n^X) = \mathrm{E}(U_n^Y)$ and that (1) is a surrogate for (2), we then have from Tunno (2015) that

$$T_1 \overset{H_0}{=} \frac{U_n^X - U_n^Y}{\sqrt{\mathrm{Var}(U_n^X) + \mathrm{Var}(U_n^Y)}} \overset{D}{\to} \mathrm{N}(0,1). \tag{4}$$

Thus, the *bounded area test of size* α tells us to reject the null hypothesis in (3) if the magnitude of our test statistic in (4) exceeds $z_{\alpha/2}$, where $z_{\alpha/2}$ is the standard normal critical value with area $\alpha/2$ to its right. That is, we reject H_0 if $|T_1| > z_{\alpha/2}$.

2.2. Arc length test

The arc length test is very similar to the bounded area test in that it utilizes a specific geometric feature of a time series plot. The arc length of time series $\{X_t\}$ observed over $t = 1, 2, \ldots, n$ is equal to

$$V_n^X = \sum_{t=2}^{n} \sqrt{1 + (X_t - X_{t-1})^2} = \sum_{t=2}^{n} S_t^X$$

and is simply the sum of the lengths of the $n - 1$ line segments connecting adjacent points on a scatter plot (see Figures 3 and 4). Tunno, Gallagher, and Lund (2012) showed that if two independent, stationary ARMA processes with finite fourth moments are observed over the same period, then a significant difference between their arc lengths implies a significant difference between their autocovariance structures.

Now assume that $\{X_t\}$ follows (1). If we again treat $\{X_t\}$ as being mean-zero, then the process is stationary, which makes $\{S_t^X\}$ stationary as well. Thus, we have

$$\mathrm{Var}(V_n^X) = \mathrm{Var}\left(\sum_{t=2}^{n} S_t^X\right) = (n-1)\gamma_{S^X}(0) + 2\sum_{h=1}^{n-2}(n-1-h)\gamma_{S^X}(h),$$

where $\gamma_{S^X}(h) = \mathrm{Cov}(S_t^X, S_{t+h}^X)$. If $\{Y_t\}$ also follows (1), then V_n^Y and its associated functionals are defined analogously.

If $\{X_t\}$ and $\{Y_t\}$ are independent of one another, then given samples $X_1, X_2, \ldots, X_n$ and $Y_1, Y_2, \ldots, Y_n$, a normalized test statistic for (3) is equal to

$$T_2 = \frac{V_n^X - V_n^Y - \mathrm{E}(V_n^X - V_n^Y)}{\sqrt{\mathrm{Var}(V_n^X - V_n^Y)}} = \frac{V_n^X - V_n^Y - \left(\mathrm{E}(V_n^X) - \mathrm{E}(V_n^Y)\right)}{\sqrt{\mathrm{Var}(V_n^X) + \mathrm{Var}(V_n^Y)}}.$$

Under the assumptions that the null hypothesis in (3) implies $\mathrm{E}(V_n^X) = \mathrm{E}(V_n^Y)$ and that (1) is a surrogate for (2), we then have from Tunno, Gallagher, and Lund (2012) that

$$T_2 \overset{H_0}{=} \frac{V_n^X - V_n^Y}{\sqrt{\mathrm{Var}(V_n^X) + \mathrm{Var}(V_n^Y)}} \overset{D}{\to} \mathrm{N}(0,1). \tag{5}$$

Thus, the *arc length test of size* α tells us to reject the null hypothesis in (3) if the magnitude of our test statistic in (5) exceeds $z_{\alpha/2}$, where as before $z_{\alpha/2}$ is the standard normal critical value with area $\alpha/2$ to its right. That is, we reject H_0 if $|T_2| > z_{\alpha/2}$.

2.3. Absolute lag-one test

The absolute lag-one test is similar to both the bounded area and arc length tests in that the test statistic is once again a function of the lag-one difference $X_t - X_{t-1}$. Specifically, for time series $\{X_t\}$ observed over $t = 1, 2, \ldots, n$, we have

$$W_n^X = \sum_{t=2}^{n} |X_t - X_{t-1}|^k = \sum_{t=2}^{n} P_t^X,$$

where $k \geq 1$.

Now assume that $\{X_t\}$ follows (1). If we again treat $\{X_t\}$ as being mean-zero, then the process is stationary, which makes $\{P_t^X\}$ stationary as well. Thus, we have

$$\mathrm{Var}(W_n^X) = \mathrm{Var}\left(\sum_{t=2}^{n} P_t^X\right) = (n-1)\gamma_{P^X}(0) + 2\sum_{h=1}^{n-2}(n-1-h)\gamma_{P^X}(h),$$

where $\gamma_{P^X}(h) = \mathrm{Cov}(P_t^X, P_{t+h}^X)$. If $\{Y_t\}$ also follows (1), then W_n^Y and its associated functionals are defined analogously.

If $\{X_t\}$ and $\{Y_t\}$ are independent of one another, then given samples $X_1, X_2, \ldots, X_n$ and $Y_1, Y_2, \ldots, Y_n$, a normalized test statistic for (3) is equal to

$$T_3 = \frac{W_n^X - W_n^Y - \mathrm{E}(W_n^X - W_n^Y)}{\sqrt{\mathrm{Var}(W_n^X - W_n^Y)}} = \frac{W_n^X - W_n^Y - \left(\mathrm{E}(W_n^X) - \mathrm{E}(W_n^Y)\right)}{\sqrt{\mathrm{Var}(W_n^X) + \mathrm{Var}(W_n^Y)}}.$$

Under the assumptions that the null hypothesis in (3) implies $\mathrm{E}(W_n^X) = \mathrm{E}(W_n^Y)$ and that (1) is a surrogate for (2), we then have from Theorem 2.1 below that

$$T_3 \overset{H_0}{=} \frac{W_n^X - W_n^Y}{\sqrt{\mathrm{Var}(W_n^X) + \mathrm{Var}(W_n^Y)}} \overset{D}{\to} \mathrm{N}(0,1). \tag{6}$$

Thus, the *absolute lag-one test of size* α tells us to reject the null hypothesis in (3) if the magnitude of our test statistic in (6) exceeds $z_{\alpha/2}$, where as before $z_{\alpha/2}$ is the standard normal critical value with area $\alpha/2$ to its right. That is, we reject H_0 if $|T_3| > z_{\alpha/2}$.

Note that while the mean-zero assumption is necessary for the bounded area test to be meaningful, the arc length and absolute lag-one tests can be run for any constant mean. That is, if (1) happened to have an intercept term, we would subtract it off from all observations first before running the bounded area test, but such a step would be unnecessary for both the arc length and absolute lag-one tests. Observe also that in practice, the variances in the denominators of T_1, T_2, and T_3 will be unknown, but as long as they are replaced with consistent estimators, all three tests are unaffected.

Theorem 2.1. *Let $\{X_t\}$ and $\{Y_t\}$ each follow model (2) and be independent of one another. Then, under the assumption of the null hypothesis in (3), the test statistic in (6) converges in distribution to the standard normal. That is, $T_3 \overset{D}{\to} \mathrm{N}(0,1)$ when H_0 is true.*

Proof: We will use Corollary 1 of Theorem 1 from Wu (2002). First, assume that $\{X_t\}$ follows (2), in which case $\{X_t\}$ is a causal linear process. That is,

$$X_t = \sum_{i=0}^{\infty} \psi_i \epsilon_{t-i}$$

where the ψ_i's are absolutely summable. Furthermore, pick some $k \geq 1$ and then assume that $E(X_t^s)<\infty$, where s is the smallest integer greater than or equal to $2k$ (i.e., $s = \lceil 2k \rceil$).

Now, consider the following objects connected to sample $X_1, X_2, ..., X_n$:

A. $X_n = \sum_{i=0}^{\infty} \psi_i \epsilon_{n-i}$
B. $X_{n,-} = \sum_{i=n}^{\infty} \psi_i \epsilon_{n-i}$
C. $P_n^X = |X_n - X_{n-1}|^k$
D. $P_{n,-}^X = |X_{n,-} - X_{n-1,-}|^k$
E. $K(X_{n-1}, X_n) = P_n^X - \mathrm{E}(P_n^X)$
F. $K(X_{n-1,-}, X_{n,-}) = P_{n,-}^X - \mathrm{E}(P_{n,-}^X)$

Observe that

$$\mathrm{E}\Big(K(X_{n-1,-}, X_{n,-})\Big)^2 \leq \mathrm{E}(P_{n,-}^X)^2 \leq \nu\ \mathrm{E}(X_{n,-})^2$$

for some $\nu > 0$, since $|X_{n,-} - X_{n-1,-}|<\infty$. If $||\cdot||$ denotes the $\mathcal{L}^2$-norm, it follows that

$$\begin{aligned}
\sum_{n=2}^{\infty} \frac{||K(X_{n-1,-}, X_{n,-})||}{\sqrt{n}} &\leq \nu^{1/2} \sum_{n=2}^{\infty} \frac{||X_{n,-}||}{\sqrt{n}} \\
&= \nu^{1/2} \sum_{n=2}^{\infty} \sqrt{\mathrm{E}\left(\sum_{i=n}^{\infty} \psi_i \epsilon_{n-i}\right)^2 / n} \\
&\leq \nu^{1/2} \sum_{n=2}^{\infty} \sqrt{\mathrm{E}\left(\sum_{i=n}^{\infty} |\psi_i| \sqrt{n}\right)^2 / n} \\
&= \nu^{1/2} \sum_{n=2}^{\infty} \sum_{i=n}^{\infty} |\psi_i| < \infty,
\end{aligned}$$

since for any causal ARMA process, we have $|\psi_k| \leq Cr^k$ for some $C > 0$ and $r \in (0, 1)$. Then, by Corollary 1 of Theorem 1 from Wu (2002), we have

$$L_K^X = \frac{1}{\sqrt{n}} \sum_{t=2}^{n} K(X_{t-1}, X_t) = \frac{W_n^X - \mathrm{E}(W_n^X)}{\sqrt{n}} \xrightarrow{D} \mathrm{N}(0, \sigma_K^2),$$

where $\sigma_K^2 = \lim_{n\to\infty} \mathrm{Var}(L_K^X)$. An analogous result holds for $\{Y_t\}$. Thus, we have

$$\frac{L_K^X - L_K^Y}{\sqrt{\mathrm{Var}(L_K^X - L_K^Y)}} \overset{H_0}{=} \frac{W_n^X - W_n^Y}{\sqrt{\mathrm{Var}(W_n^X) + \mathrm{Var}(W_n^Y)}} \xrightarrow{D} \mathrm{N}(0, 1)$$

by Slutsky's theorem and the independence of $\{X_t\}$ and $\{Y_t\}$. □

In practice, it is probably best to choose a k value for the absolute lag-one test such that $k \in [1, 2]$. In Theorem 2.1 above, when k is larger than 2, you are forced to assume that your process must have finite moments of order more than four, which is not always realistic. The simulations in the next section also reveal that as k increases beyond 2, the ability of W_n^X or W_n^Y to accurately assess the influence of lag-one differences becomes diminished.

3. Simulations

This section compares the type I error and power of the bounded area, arc length, and absolute lag-one tests for testing (3) at level $\alpha = 0.05$. In all figures, these tests will be abbreviated as AR, AL, and AB, respectively. For each figure, series of length $n = 1,000$ were generated while 10,000 independent simulations were conducted to estimate the error and power values. $\{X_t\}$ and $\{Y_t\}$ are independent of each other and both follow (1). Z_t^X and Z_t^Y denote the error terms for $\{X_t\}$ and $\{Y_t\}$, respectively, and are i.i.d. standard normal unless stated otherwise. The normality of the errors make process moments of all orders finite.

This section is henceforth divided up into subsections that correspond to different k-values for the absolute lag-one test. For each of these k-values, the following four signal scenarios will be explored:

	Error	Power
(S_1)	$X_t = A\sin t + Z_t^X$ $Y_t = A\sin t + Z_t^Y$ $-2 \le A \le 2$	$X_t = Z_t^X$ $Y_t = A\sin t + Z_t^Y$ $-2 \le A \le 2$
(S_2)	$X_t = \sin t + A\cos t + Z_t^X$ $Y_t = \sin t + A\cos t + Z_t^Y$ $-2 \le A \le 2$	$X_t = \sin t + Z_t^X$ $Y_t = \sin t + A\cos t + Z_t^Y$ $-2 \le A \le 2$
(S_3)	$X_t = \sin(t + A) + \cos t + Z_t^X$ $Y_t = \sin(t + A) + \cos t + Z_t^Y$ $-2 \le A \le 2$	$X_t = \sin t + \cos t + Z_t^X$ $Y_t = \sin(t + A) + \cos t + Z_t^Y$ $-2 \le A \le 2$
(S_4)	$X_t = \sin t + Z_t^X$ $Y_t = \sin t + Z_t^Y$ $\{Z_t^X\} \overset{\text{iid}}{\sim} N(0, \sigma^2)$ $\{Z_t^Y\} \overset{\text{iid}}{\sim} N(0, \sigma^2)$ $1 \le \sigma \le 3$	$X_t = \sin t + Z_t^X$ $Y_t = \sin t + Z_t^Y$ $\{Z_t^X\} \overset{\text{iid}}{\sim} N(0, 4)$ $\{Z_t^Y\} \overset{\text{iid}}{\sim} N(0, \sigma^2)$ $1 \le \sigma \le 3$

3.1. $k = 1$

Figures 6–9 correspond to scenarios (S_1) through (S_4), respectively. In the first three scenarios, all three tests have low error and increase power as A deviates from zero, especially the bounded area test. In the fourth one, all three tests have low error and increase power as σ deviates from two.

3.2. $k = 2$

Although not shown here, the simulation results for scenarios (S_1) through (S_4) when $k = 2$ are indistinguishable from those when $k = 1$.

3.3. $k = 4$

Figures 10–13 correspond to scenarios (S_1) through (S_4), respectively. In scenarios (S_1) through (S_3), increasing k to 4 causes the absolute lag-one test to lose some of its earlier power.

3.4. $k = 6$

Although not shown here, the simulation results for scenarios (S_1) through (S_4) reveal that the absolute lag-one test loses even more power in the first three scenarios when k increases to 6.

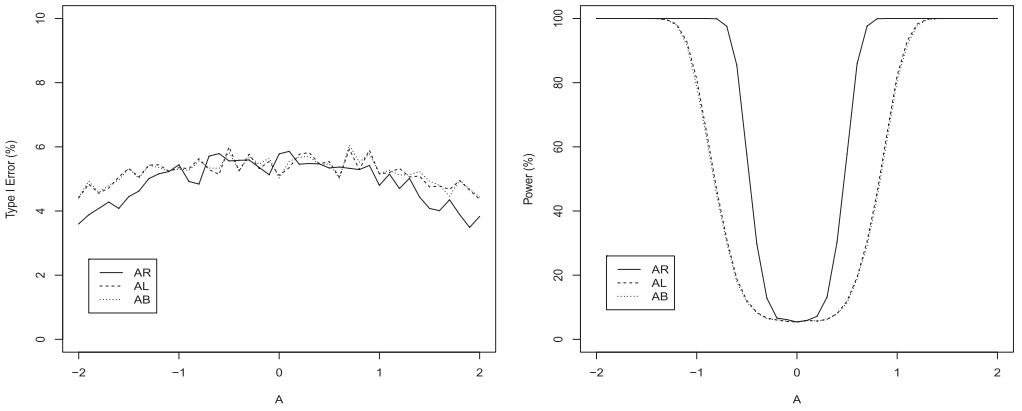

Figure 6. Error (left) and power (right) for scenario (S_1) when k = 1.

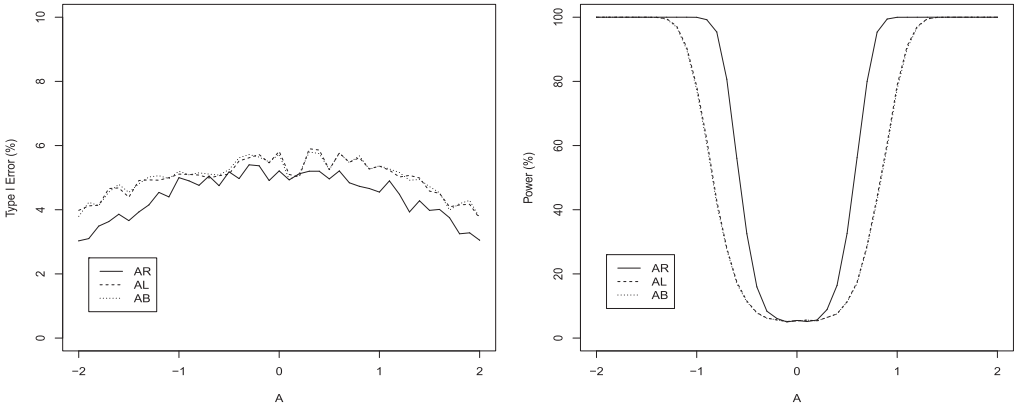

Figure 7. Error (left) and power (right) for scenario (S_2) when k = 1.

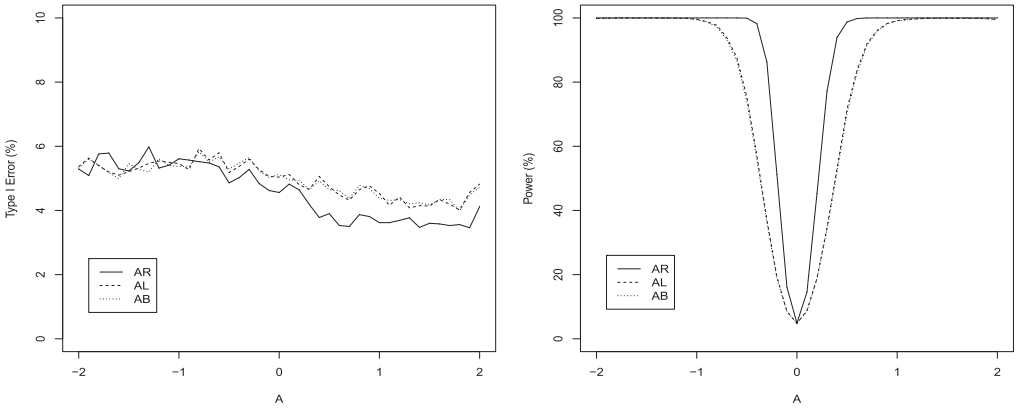

Figure 8. Error (left) and power (right) for scenario (S_3) when k = 1.

3.5. k = 9

Figures 14–17 correspond to scenarios (S_1) through (S_4), respectively. In all four scenarios, a *k*-value of 9 leaves the absolute lag-one test with very little power.

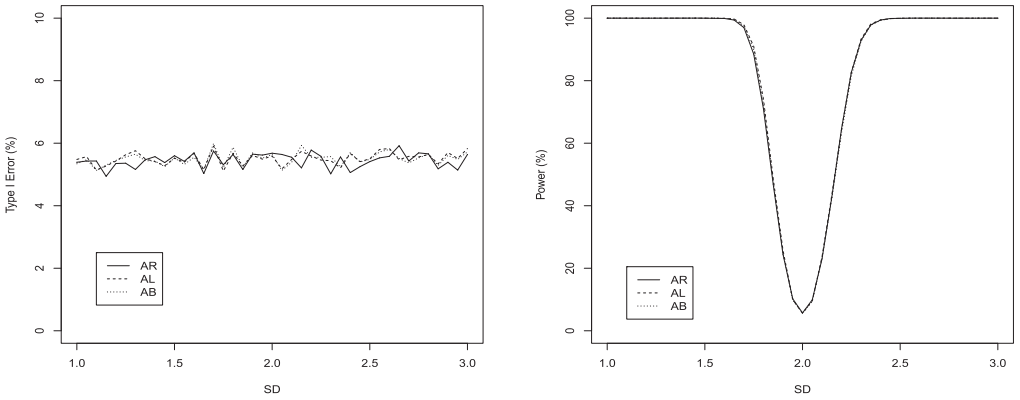

Figure 9. Error (left) and power (right) for scenario (S_4) when $k = 1$.

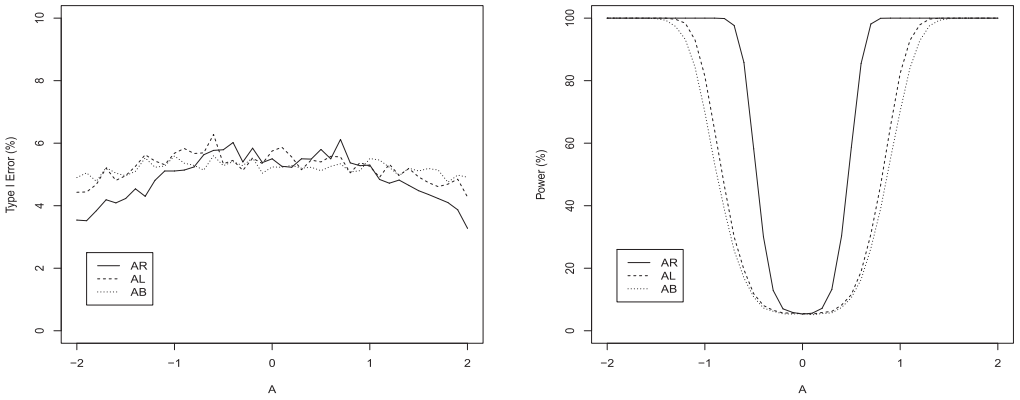

Figure 10. Error (left) and power (right) for scenario (S_1) when $k = 4$.

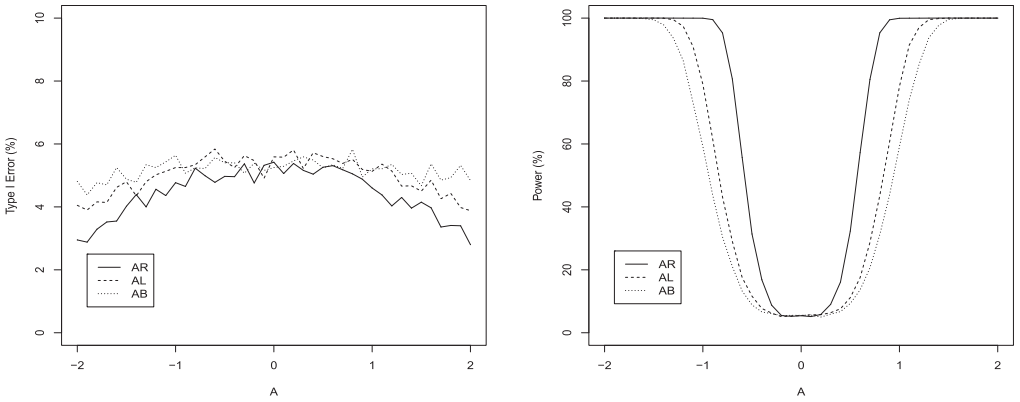

Figure 11. Error (left) and power (right) for scenario (S_2) when $k = 4$.

4. Application

Signal discrimination has a wide variety of applications in fields ranging from telecommunications to psychology to quality control. One particularly interesting application

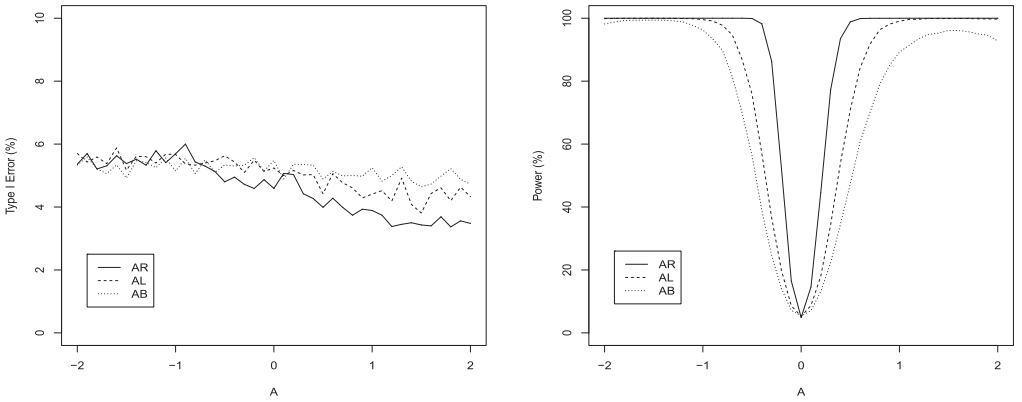

Figure 12. Error (left) and power (right) for scenario (S_3) when k = 4.

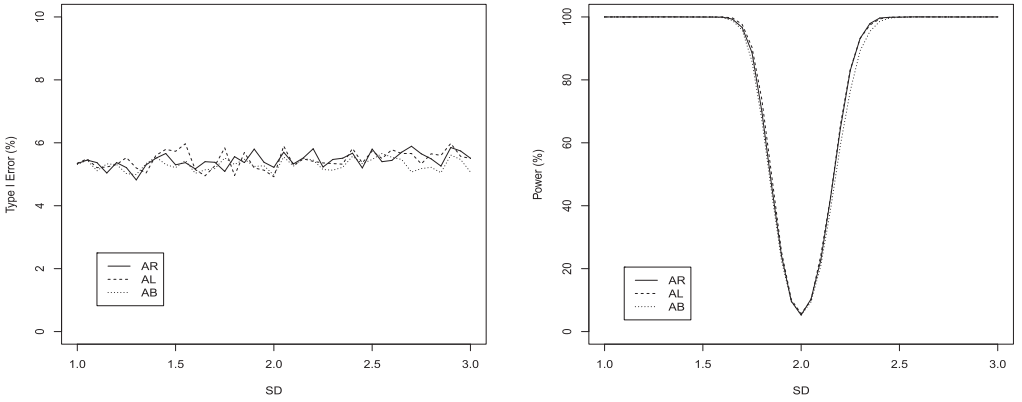

Figure 13. Error (left) and power (right) for scenario (S_4) when k = 4.

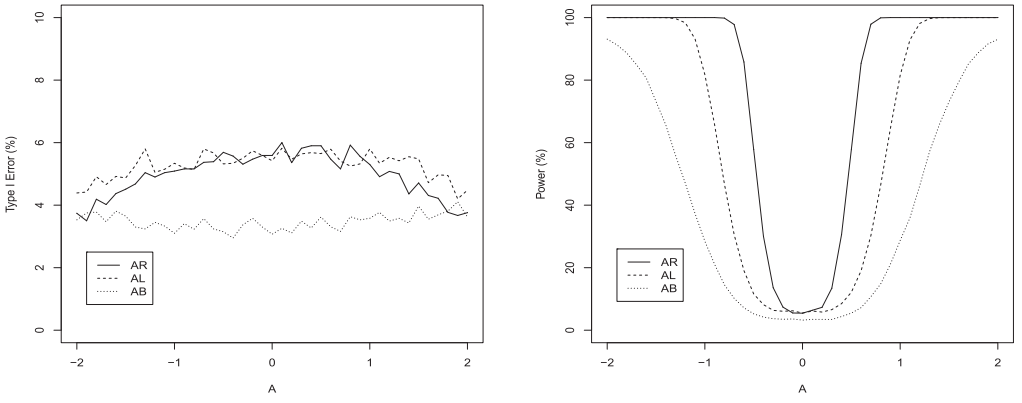

Figure 14. Error (left) and power (right) for scenario (S_1) when k = 9.

comes from military intelligence and involves monitoring seismic activity in countries thought to be engaged in underground nuclear testing. The waveform is analyzed to see if it is truly nuclear in nature or simply the result of an earthquake or mining explosion. See Shumway (2003) and Kakizawa, Shumway, and Taniguchi (1998).

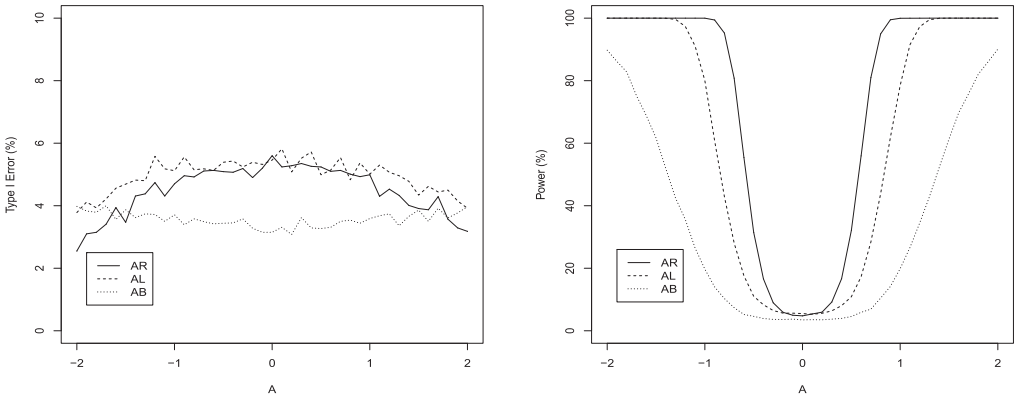

Figure 15. Error (left) and power (right) for scenario (S_2) when $k = 9$.

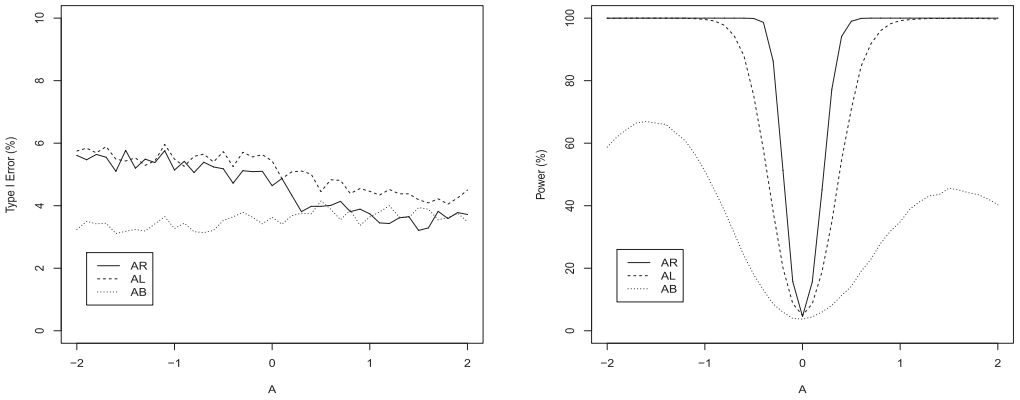

Figure 16. Error (left) and power (right) for scenario (S_3) when $k = 9$.

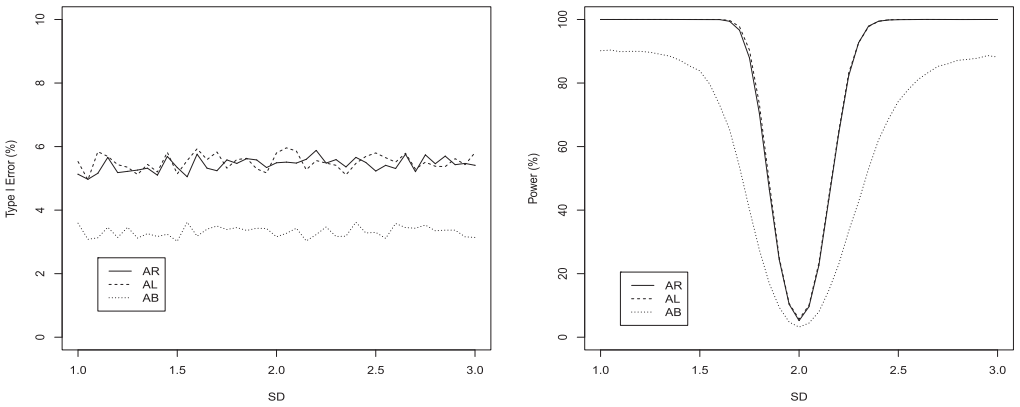

Figure 17. Error (left) and power (right) for scenario (S_4) when $k = 9$.

Another important application involves functional magnetic resonance imaging (fMRI). Figure 18 shows eight realizations of blood oxygenation-level dependent (BOLD) signal intensities corresponding to various locations in the brain. Cortex 1 and Cortex 2 correspond, respectively, to the contralateral and ipsilateral primary

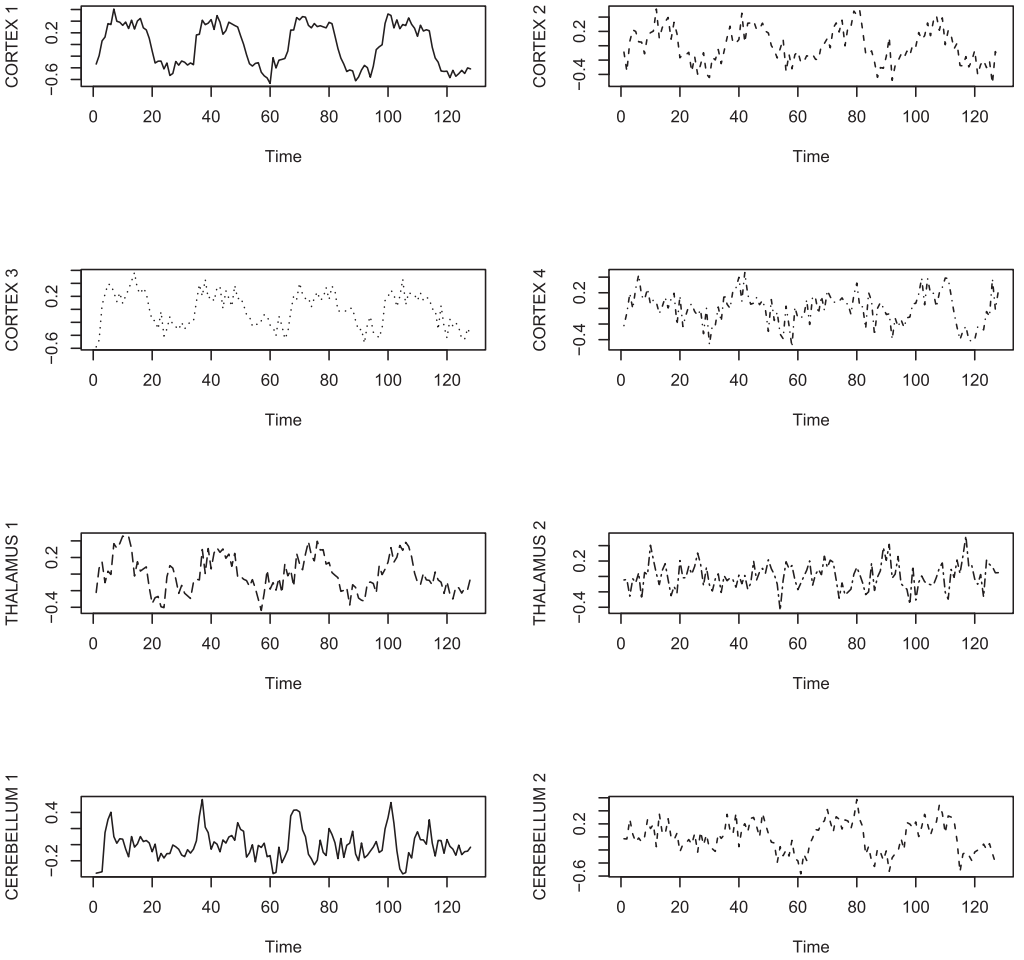

Figure 18. Eight realizations of blood oxygenation-level dependent (BOLD) signal intensities corresponding to various locations in the brain.

somatosensory cortex. Cortex 3 and Cortex 4 correspond, respectively, to the contralateral and ipsilateral secondary somatosensory cortex. Thalamus 1 and Thalamus 2 correspond, respectively, to the contralateral and ipsilateral thalamus. Cerebellum 1 and Cerebellum 2 correspond, respectively, to the contralateral and ipsilateral cerebellum.

Each signal is the average of individual signals for five different subjects, all of which are in phase. Each subject was given periodic brushing on the hand. Specifically, the stimulus was applied for 32 seconds and then stopped for 32 seconds, which makes each signal period 64 seconds. The sampling rate was one observation every 2 seconds for 256 seconds, which makes the sample size $n = 128$.

Table 1 shows the magnitudes of test statistic T_1 from (4) when the bounded area test is applied pairwise to all eight signals. Table 2 shows the magnitudes of test statistic T_2 from (5) when the arc length test is applied pairwise to all eight signals. Table 3 shows the magnitudes of test statistic T_3 from (6) when the absolute lag-one test with $k = 2$ is applied pairwise to all eight signals.

Table 1. The magnitudes of test statistic T_1 when the bounded area test is applied pairwise to all eight signals.

	CO_1	CO_2	CO_3	CO_4	TH_1	TH_2	CE_1	CE_2
CO_1	0	6.117	4.823	7.599	6.978	11.580	8.340	5.524
CO_2	6.117	0	1.321	2.097	1.180	5.260	3.133	0.265
CO_3	4.823	1.321	0	3.268	2.424	6.687	4.233	1.369
CO_4	7.599	2.097	3.268	0	0.936	2.072	1.058	1.537
TH_1	6.978	1.180	2.424	0.936	0	3.477	1.993	0.735
TH_2	11.580	5.260	6.687	2.072	3.477	0	0.591	3.701
CE_1	8.340	3.133	4.233	1.058	1.993	0.591	0	2.461
CE_2	5.524	0.265	1.369	1.537	0.735	3.701	2.461	0

Table 2. The magnitudes of test statistic T_2 when the arc length test is applied pairwise to all eight signals.

	CO_1	CO_2	CO_3	CO_4	TH_1	TH_2	CE_1	CE_2
CO_1	0	3.874	2.516	4.146	0.731	4.288	1.169	3.812
CO_2	3.874	0	1.306	1.127	2.876	0.398	2.475	0.242
CO_3	2.516	1.306	0	2.193	1.602	1.705	1.198	1.468
CO_4	4.146	1.127	2.193	0	3.429	0.796	3.117	0.880
TH_1	0.731	2.876	1.602	3.429	0	3.266	0.395	2.925
TH_2	4.288	0.398	1.705	0.796	3.266	0	2.866	0.134
CE_1	1.169	2.475	1.198	3.117	0.395	2.866	0	2.555
CE_2	3.812	0.242	1.468	0.880	2.925	0.134	2.555	0

Table 3. The magnitudes of test statistic T_3 when the absolute lag-one test with $k = 2$ is applied pairwise to all eight signals.

	CO_1	CO_2	CO_3	CO_4	TH_1	TH_2	CE_1	CE_2
CO_1	0	3.839	2.485	4.101	0.706	4.241	1.150	3.756
CO_2	3.839	0	1.316	1.114	2.888	0.386	2.479	0.225
CO_3	2.485	1.316	0	2.187	1.608	1.704	1.195	1.459
CO_4	4.101	1.114	2.187	0	3.421	0.793	3.104	0.881
TH_1	0.706	2.888	1.608	3.421	0	3.269	0.403	2.914
TH_2	4.241	0.386	1.704	0.793	3.269	0	2.861	0.139
CE_1	1.150	2.479	1.195	3.104	0.403	2.861	0	2.538
CE_2	3.756	0.225	1.459	0.881	2.914	0.139	2.538	0

If our significance level is $\alpha = 0.05/28$ (Bonferroni), then we reject the null hypothesis of equal wave structures if $|T_1|, |T_2|$, or $|T_3|$ exceeds $z_{(0.05/28)/2} = 3.124$, depending on which test we use. All three tests suggest, for example, that Cortex 1 (CO_1) and Thalamus 2 (TH_2) have different waveforms. All three tests also suggest that Cortex 2 (CO_2) and Cortex 3 (CO_3) have similar waveforms. Figure 19 gives clear visual confirmation of these two conclusions.

The three tests do not always agree, however. For example, the bounded area test suggests that Thalamus 2 (TH_2) and Cerebellum 2 (CE_2) have different waveforms while both the the arc length and absolute lag-one tests conclude that they are similar. Conversely, the bounded area test suggests that Thalamus 1 (TH_1) and Cortex 4 (CO_4) have similar waveforms while both the arc length and absolute lag-one tests conclude that they are different. Figure 20 seems to give more credence to the conclusions of the bounded area test. This is not particularly surprising since the simulations in the previous section reveal the bounded area test to be more likely than the other two tests to reject a false null hypothesis and hence less likely to accept one.

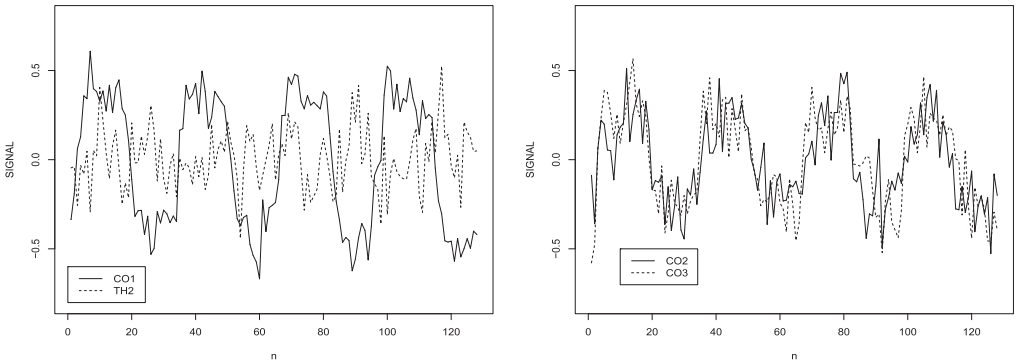

Figure 19. (Left) Superimposed waveforms for Cortex 1 (CO_1) and Thalamus 2 (TH_2). (Right) Superimposed waveforms for Cortex 2 (CO_2) and Cortex 3 (CO_3).

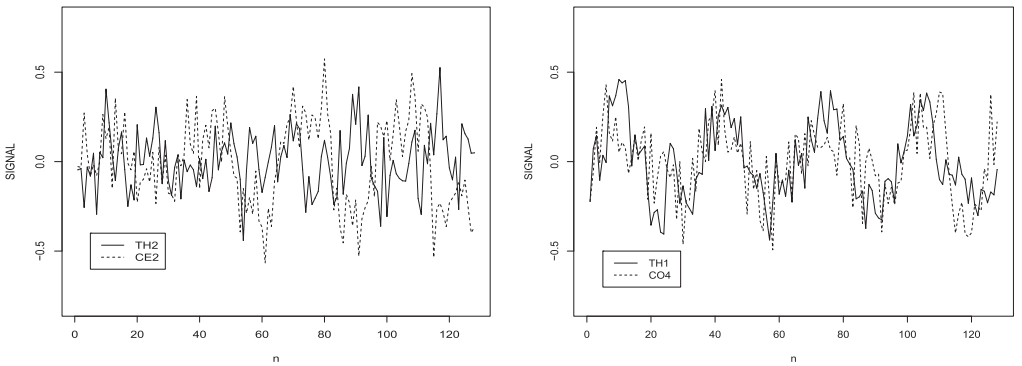

Figure 20. (Left) Superimposed waveforms for Thalamus 2 (TH_2) and Cerebellum 2 (CE_2). (Right) Superimposed waveforms for Thalamus 1 (TH_1) and Cortex 4 (CO_4).

For more information on the data set used in this section, see Chapter 1 of Shumway and Stoffer (2006). To access the raw data itself, go to http://www.stat.pitt.edu/stoffer/tsa2. To see a nice example of how an in-depth fMRI study can reveal correlations between tactile sensation and the brain, see Ackerly et al. (2012).

5. Closing remarks and extensions

This article reveals the bounded area, arc length, and absolute lag-one tests to be effective at signal discrimination, especially the bounded area test. Overall, it is more powerful and has slightly lower error, with the exception of certain cases involving signal scenario (S_4). Since none of these tests require any denoising, it is natural at this point to ask whether any smoothing or noise reduction would actually augment the results even more.

Figures 21–24 repeat the same simulations as those in Figures 6–9, respectively, but this time a Savitzky-Golay filter is applied to the data first. Specifically, X_t gets replaced with

$$\frac{-3X_{t-2} + 12X_{t-1} + 17X_t + 12X_{t+1} - 3X_{t+2}}{35} \quad t = 1, 2, \ldots, n,$$

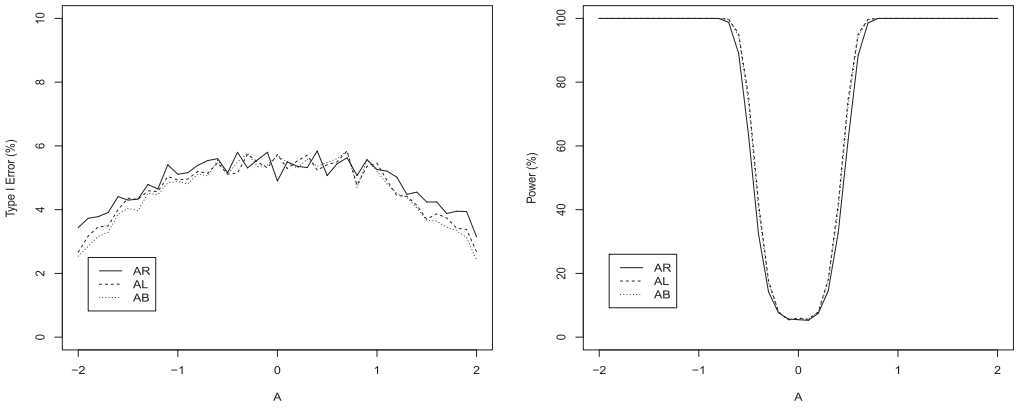

Figure 21. Error (left) and power (right) for scenario (S_1) when $k = 1$ using a Savitzky-Golay filter. Compare to Figure 6.

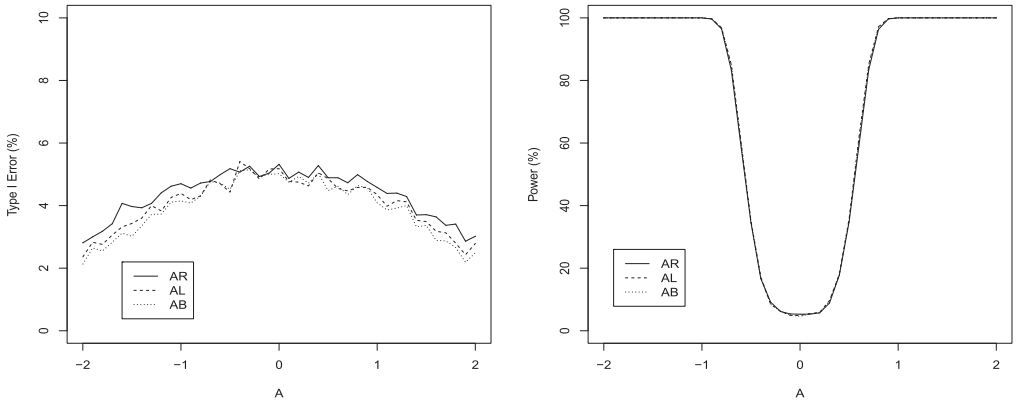

Figure 22. Error (left) and power (right) for scenario (S_2) when $k = 1$ using a Savitzky-Golay filter. Compare to Figure 7.

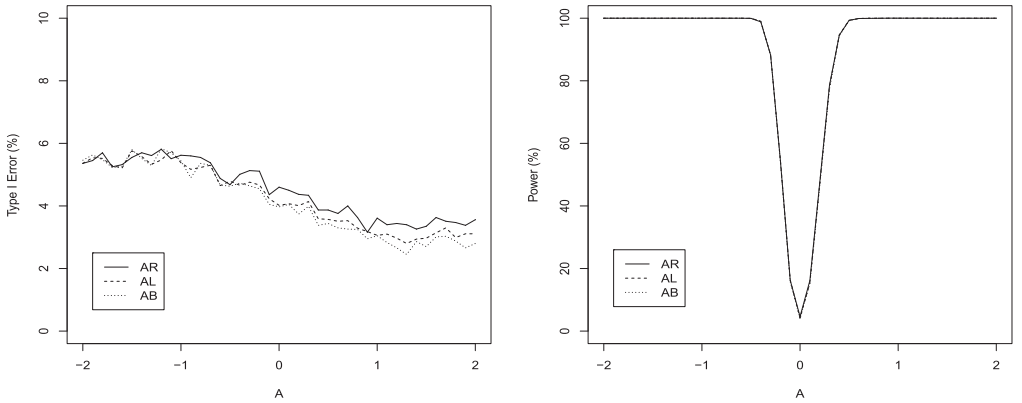

Figure 23. Error (left) and power (right) for scenario (S_3) when $k = 1$ using a Savitzky-Golay filter. Compare to Figure 8.

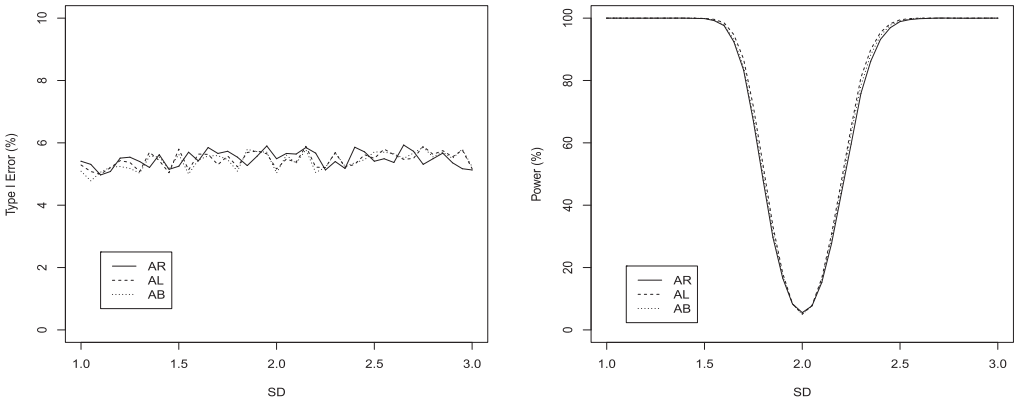

Figure 24. Error (left) and power (right) for scenario (S_4) when k = 1 using a Savitzky-Golay filter. Compare to Figure 9.

where we define X_{-1} and X_0 as X_1 and X_{n+1} and X_{n+2} as X_n. The filter is applied to Y_t in an analogous fashion. See Savitzky and Golay (1964).

All four figures reveal that the Savitzky-Golay filter helps improve the performance of both the arc length and absolute lag-one tests. The error of these two tests decreases slightly while the power either increases or stays the same. Interestingly, the bounded area test is completely unaffected one way or the other by the filter. All three tests now behave virtually the same. To get some insight into why this may be the case, we define the following objects:

$$\begin{aligned}
T_{1,n,b} &= \text{num. of } T_1 \text{ before filter} \\
T_{1,n,a} &= \text{num. of } T_1 \text{ after filter} \\
T_{2,n,b} &= \text{num. of } T_2 \text{ before filter} \\
T_{2,n,a} &= \text{num. of } T_2 \text{ after filter} \\
T_{3,n,b} &= \text{num. of } T_3 \text{ before filter} \\
T_{3,n,a} &= \text{num. of } T_3 \text{ after filter} \\
&(\text{num.} = \text{numerator})
\end{aligned}$$

$$\begin{aligned}
T_{1,d,b} &= \text{den. of } T_1 \text{ before filter} \\
T_{1,d,a} &= \text{den. of } T_1 \text{ after filter} \\
T_{2,d,b} &= \text{den. of } T_2 \text{ before filter} \\
T_{2,d,a} &= \text{den. of } T_2 \text{ after filter} \\
T_{3,d,b} &= \text{den. of } T_3 \text{ before filter} \\
T_{3,d,a} &= \text{den. of } T_3 \text{ after filter} \\
&(\text{den.} = \text{denominator})
\end{aligned}$$

Table 4 contains entries equaling the number of times (out of 5,000) both the numerator and denominator of our three test statistics increased as a result of denoising. The power version of signal scenario (S_1) was employed for values $A \in \{\pm 1, \pm 1.5, \pm 2\}$, where $n = 1{,}000$. The value $k = 2$ was used for the absolute lag-one test statistic. Clearly, smoothing significantly benefited both the arc length (T_2) and absolute lag-one (T_3) test statistics since their denominators (i.e., the variability between the two independent processes) decreased 100% of the time.

The next part of this section presents an extension involving a continuous uniform random variable. It is well known that if we replace the a_i's with uniform random variables distributed over the interval $[0, 2\pi]$ in (1), then the resulting process is no longer approximately mean-zero stationary, but exactly so. Specifically, if $U_1, U_2, \ldots, U_m \overset{\text{iid}}{\sim} \text{Uniform}[0, 2\pi]$, then

$$X_t = \sum_{i=1}^{m} A_i \sin(\lambda_i t + U_i) + Z_t \quad t = 0, \pm 1, \pm 2, \ldots$$

Table 4. The number of times (out of 5,000) both the numerator and denominator of our three test statistics increased as a result of denoising for signal scenario (S_1) with $A \in \{\pm 1, \pm 1.5, \pm 2\}$, k = 2 and n = 1,000.

	−2	−1.5	−1	1	1.5	2
$T_{1,n,b} - T_{1,n,a}$	3889	4544	4295	4233	4554	3898
$T_{1,d,b} - T_{1,d,a}$	668	1589	2637	2668	1591	737
$T_{2,n,b} - T_{2,n,a}$	4998	4928	4302	4306	4927	4994
$T_{2,d,b} - T_{2,d,a}$	0	0	0	0	0	0
$T_{3,n,b} - T_{3,n,a}$	139	774	1592	1612	729	153
$T_{3,d,b} - T_{3,d,a}$	0	0	0	0	0	0

defines a process such that $\mathrm{E}(X_t) = 0$ and

$$\mathrm{Cov}(X_t, X_{t+h}) = \begin{cases} \frac{1}{2}\sum_{i=1}^{m} A_i^2 + \sigma^2 & h = 0 \\ \frac{1}{2}\sum_{i=1}^{m} A_i^2 \cos(\lambda_i h) & h \neq 0 \end{cases}.$$

For more details, see Sec. 4.1 of Woodward, Gray, and Elliott (2012).

If we tweak the model yet again to become

$$X_t = \sum_{i=1}^{m} A_i \cos(\lambda_i t^2 + b_i t + U_i) + Z_t \quad t = 0, \pm 1, \pm 2, \ldots,$$

where the b_i's are constants for all $i = 1, 2, \ldots, m$, we have what is called a *generalized linear chirp* (GLC) process. This is also mean-zero stationary and gets its name from the fact that the instantaneous frequency changes linearly in time. Linear chirps have been used extensively to model a wide variety of physical signals such as radar, sonar, and whale clicks. See Robertson, Gray, and Woodward (2010).

For simulation purposes, we will force the uniform random variables in the above GLC process to become stochastic and vary in time, and thus $\{X_t\}$ and $\{Y_t\}$ will be defined as follows:

$$X_t = \sum_{i=1}^{m} A_i \cos(\lambda_i t^2 + b_i t + U_{i,t}^X) + Z_t^X$$
$$Y_t = \sum_{i=1}^{m} A_i \cos(\lambda_i t^2 + b_i t + U_{i,t}^Y) + Z_t^Y$$

We will also assume that the uniform random variables are uncorrelated with respect to time.

Figures 25–27 reveal the error and power of the bounded area, arc length, and absolute lag-one tests with $k = 1$ for signal scenarios (S_5) through (S_7), respectively. These new scenarios involve linear chirps and are outlined below. In scenarios (S_5) and (S_6), all three tests have low error and increase power as A deviates from zero, with the bounded area test having a slight power advantage. In scenario (S_7), all three tests have low error and increase power as σ deviates from two, with the bounded area test once again having a slight power advantage.

	Error	Power
(S_5)	$X_t = A\cos(t^2 + t + U^X_{1,t}) + Z^X_t$ $Y_t = A\cos(t^2 + t + U^Y_{1,t}) + Z^Y_t$ $-2 \le A \le 2$	$X_t = Z^X_t$ $Y_t = A\cos(t^2 + t + U^Y_{1,t}) + Z^Y_t$ $-2 \le A \le 2$
(S_6)	$X_t = \cos(t^2 + t + U^X_{1,t})$ $+A\sin(t^2 + t + U^X_{2,t}) + Z^X_t$ $Y_t = \cos(t^2 + t + U^Y_{1,t})$ $+A\sin(t^2 + t + U^Y_{2,t}) + Z^Y_t$ $-2 \le A \le 2$	$X_t = \cos(t^2 + t + U^X_{1,t}) + Z^X_t$ $Y_t = \cos(t^2 + t + U^Y_{1,t})$ $+A\sin(t^2 + t + U^Y_{2,t}) + Z^Y_t$ $-2 \le A \le 2$
(S_7)	$X_t = \cos(t^2 + t + U^X_{1,t}) + Z^X_t$ $Y_t = \cos(t^2 + t + U^Y_{1,t}) + Z^Y_t$ $\{Z^X_t\} \overset{\text{iid}}{\sim} N(0, \sigma^2)$ $\{Z^Y_t\} \overset{\text{iid}}{\sim} N(0, \sigma^2)$ $1 \le \sigma \le 3$	$X_t = \cos(t^2 + t + U^X_{1,t}) + Z^X_t$ $Y_t = \cos(t^2 + t + U^Y_{1,t}) + Z^Y_t$ $\{Z^X_t\} \overset{\text{iid}}{\sim} N(0, 4)$ $\{Z^Y_t\} \overset{\text{iid}}{\sim} N(0, \sigma^2)$ $1 \le \sigma \le 3$

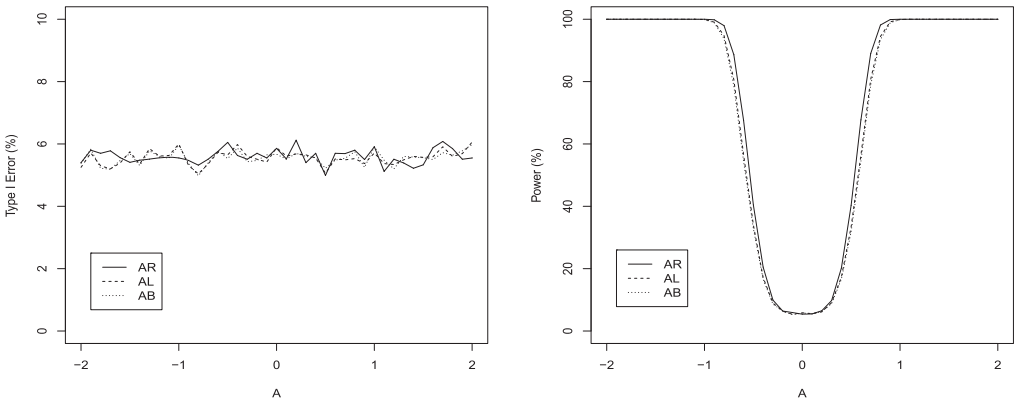

Figure 25. Error (left) and power (right) for scenario (S_5) when k = 1.

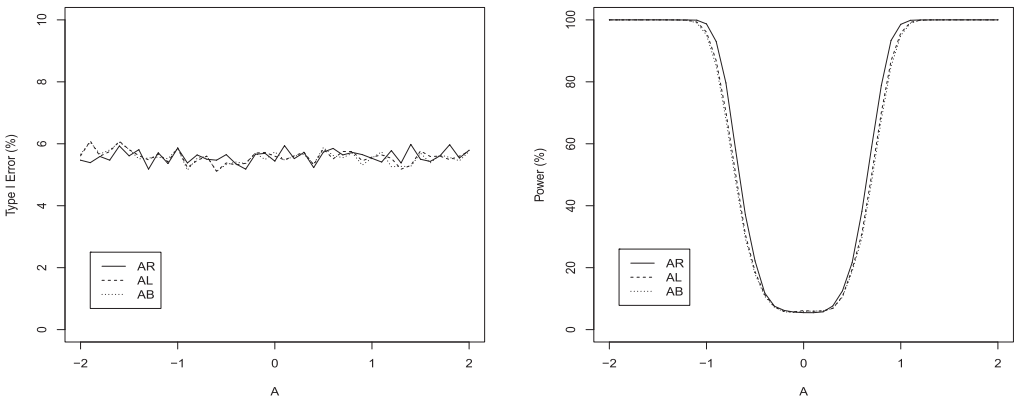

Figure 26. Error (left) and power (right) for scenario (S_6) when k = 1.

We now conclude this article with a few remarks on how to generalize our signal discrimination tests into ones that can handle multiple comparisons and not just pairwise ones. Specifically, we recommend the use of clustering to accomplish this goal. There is already precedent for using arc length to cluster financial time series - see Wickramarachchi and Tunno (2015).

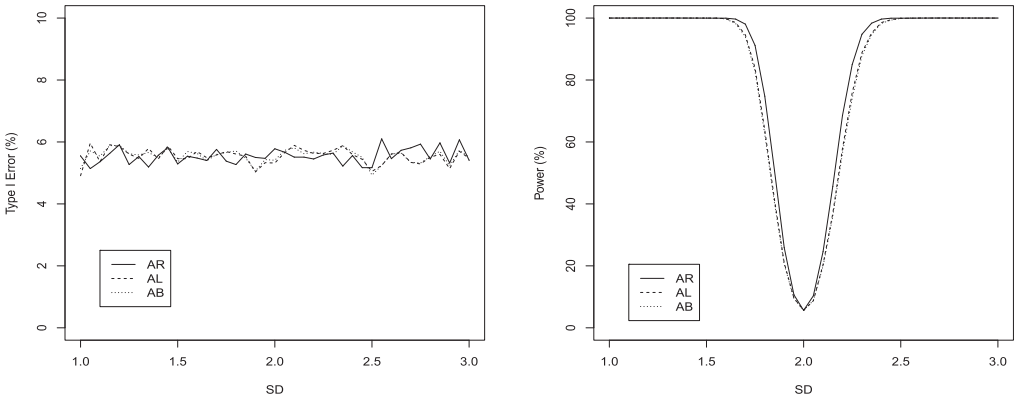

Figure 27 Error (left) and power (right) for scenario (S_7) when $k = 1$.

To see an example of how this process might work, let's assume that there is a collection of various harmonic signals following model (1) and that we have calculated the bounded area for each of them. Using the k-means++ clustering technique in conjunction with the bounded area metric, these signals can be partitioned into groups such that those within the same group have similar structures while those from different groups have dissimilar structures.

If there is reason to doubt that the clustering process has properly classified two particular signals as being either similar or dissimilar, then the pairwise bounded area test presented in this article can be invoked as a "post hoc" measure (not unlike how a Tukey test can help flesh out the results of an ANOVA test). If, on the other hand, the clustering seems appropriate, then a pairwise test can be avoided altogether. For a nice survey on recent time series clustering methods, see Aghabozorgi, Shirkhorshidi, and Wah (2015).

Acknowledgment

The authors would like to give special thanks to G. Andrew James, Ph.D., from the University of Arkansas for Medical Sciences (UAMS) for sharing his knowledge and insight on fMRI studies involving tactile sensation.

References

Ackerly, R., E. Hassan, A. Curran, J. Wessberg, H. Olausson, and F. McGlone. 2012. An fMRI study on cortical responses during active self-touch and passive touch from others. *Frontiers in Behavioral Science* 6:1–9.

Aghabozorgi, S., A. S. Shirkhorshidi, and T. Y. Wah. 2015. Time-series clustering - a decade review. *Information Systems* 53:16–38. doi:10.1016/j.is.2015.04.007.

Kakizawa, Y., R. H. Shumway, and M. Taniguchi. 1998. Discrimination and clustering for multivariate time series. *Journal of the American Statistical Association* 93 (441):328–40. doi:10.2307/2669629.

Mezer, A., Y. Yovel, O. Pasternak, T. Gorfine, and Y. Assaf. 2009. Cluster analysis of resting-state fMRI time series. *NeuroImage* 45 (4):1117–25. doi:10.1016/j.neuroimage.2008.12.015.

Robertson, S. D., H. L. Gray, and W. A. Woodward. 2010. The generalized linear chirp process. *Journal of Statistical Planning and Inference* 140 (12):3676–87. doi:10.1016/j.jspi.2010.04.033.

Savitzky, A., and M. J. E. Golay. 1964. Smoothing and differentiation of data by simplified least squares procedures. *Analytical Chemistry* 36 (8):1627–39. doi:10.1021/ac60214a047.

Shumway, R. H. 2003. Time-frequency clustering and discriminant analysis. *Statistics & Probability Letters* 63 (3):307–14. doi:10.1016/S0167-7152(03)00095-6.

Shumway, R. H., and D. S. Stoffer. 2006. *Time series analysis and its applications with R examples*, 2nd ed. New York: Springer.

Tunno, F., C. Gallagher, and R. Lund. 2012. Arc length tests for equivalent autocovariances. *Journal of Statistical Computation and Simulation* 82 (12):1799–812. doi:10.1080/00949655.2011.595717.

Tunno, F. 2015. Bounded area tests for comparing the dynamics between ARMA processes. *Communications in Statistics - Theory and Methods* 44 (18):3921–41. doi:10.1080/03610926.2013.837184.

Wickramarachchi, T., and F. Tunno. 2015. Using arc length to cluster financial time series according to risk. *Communications in Statistics: Case Studies, Data Analysis, and Applications* 1:217–25. doi:10.1080/23737484.2016.1206456.

Woodward, W. A., H. L. Gray, and A. C. Elliott. 2012. *Applied time series analysis*. Boca Raton: CRC Press.

Wu, W. B. 2002. Central limit theorems for functionals of linear processes and their applications. *Statistica Sinica* 12:635–49.